



UNIVERSITY OF LEEDS

This is a repository copy of *A personalized-model-based central aortic pressure estimation method*.

White Rose Research Online URL for this paper:  
<http://eprints.whiterose.ac.uk/108846/>

Version: Accepted Version

---

**Article:**

Jiang, S, Zhang, Z-Q [orcid.org/0000-0003-0204-3867](http://orcid.org/0000-0003-0204-3867), Wang, F et al. (1 more author)  
(2016) A personalized-model-based central aortic pressure estimation method. *Journal of Biomechanics*, 49 (16). pp. 4098-4106. ISSN 0021-9290

<https://doi.org/10.1016/j.jbiomech.2016.11.007>

---

© 2016 Elsevier Ltd. Licensed under the Creative Commons Attribution-NonCommercial-NoDerivatives 4.0 International  
<http://creativecommons.org/licenses/by-nc-nd/4.0/>

**Reuse**

Unless indicated otherwise, fulltext items are protected by copyright with all rights reserved. The copyright exception in section 29 of the Copyright, Designs and Patents Act 1988 allows the making of a single copy solely for the purpose of non-commercial research or private study within the limits of fair dealing. The publisher or other rights-holder may allow further reproduction and re-use of this version - refer to the White Rose Research Online record for this item. Where records identify the publisher as the copyright holder, users can verify any specific terms of use on the publisher's website.

**Takedown**

If you consider content in White Rose Research Online to be in breach of UK law, please notify us by emailing [eprints@whiterose.ac.uk](mailto:eprints@whiterose.ac.uk) including the URL of the record and the reason for the withdrawal request.



[eprints@whiterose.ac.uk](mailto:eprints@whiterose.ac.uk)  
<https://eprints.whiterose.ac.uk/>

# A Personalized-Model-based Central Aortic Pressure Estimation Method

Sheng Jiang<sup>1</sup>, Zhi-Qiang Zhang<sup>2</sup> Fang Wang<sup>3</sup> and Jian-Kang Wu<sup>4</sup>

<sup>1</sup>China Academy of Electronics and Information Technology, Beijing, China

<sup>2</sup>School of Electronics and Electrical Engineering, University of Leeds, UK

<sup>3</sup>Division of Cardiology, Beijing Hospital, Beijing, China

<sup>4</sup>Department of Electrical Engineering, University of Chinese Academy of Sciences, Beijing, China

Email: z.zhang3@leeds.ac.uk

## Abstract

Central Aortic Pressure (CAP) can be used to predict cardiovascular structural damage and cardiovascular events, and the development of simple, well-validated and non-invasive methods for CAP waveforms estimation is critical to facilitate the routine clinical applications of CAP. Existing widely applied methods, such as generalized transfer function (GTF-CAP) method and N-Point Moving Average (NPMA-CAP) method, are based on clinical practices, and lack a mathematical foundation. Those methods also have inherent drawback that there is no personalisation, and missing individual aortic characteristics. To overcome this pitfall, we present a personalized-model-based central aortic pressure estimation method (PM-CAP) in this paper. This PM-CAP has a mathematical foundation: a human aortic network model is proposed which is developed based on viscous fluid mechanics theory and could be personalized conveniently. Via measuring the pulse wave at the proximal and distal ends of the radial artery, the least square method is then proposed to estimate patient-specific circuit parameters. Thus the central aortic pulse wave can be obtained via calculating the transfer function between the radial artery and central aorta. An invasive validation study with 18 subjects comparing PM-CAP with direct aortic root pressure measurements during percutaneous transluminal coronary intervention was carried out at the Beijing Hospital. The experimental results show better performance of the PM-CAP method compared to the GTF-CAP method and NPMA-CAP method, which illustrates the feasibility and effectiveness of the proposed method.

## Index Terms

Central Aortic Pressure, Blood Fluid Dynamics, Human Artery Model, Transfer Function.

## I. INTRODUCTION

Central Aortic Pressure (CAP) has been widely applied to predict the cardiovascular structural damage and cardiovascular events (?). Traditionally, Blood Pressure (BP) measured over the brachial artery using a sphygmomanometer has been used to predict such damage and events directly, but the measured brachial BP can't always accurately represent the corresponding pressure in the aorta due to the influence of many factors, such as arterial stiffness, age, heart rate, body height, sex, and drug therapies. All these factors can affect the relationship between brachial pressure and CAP (?). In recent years, the standard method for CAP measurement is the direct measurement of aortic root pressures using a pressure transducer introduced into the aortic root at the time of percutaneous transluminal coronary intervention (?). This method can provide accurate CAP measurement for individuals, but it is invasive and unsuitable for routine clinical practices; therefore, the development of simple, well-validated methods for non-invasive CAP derivation is critical to facilitate routine clinical applications.

Thus far, some ad-hoc methods have been proposed for non-invasive CAP estimation. For example, ? proposed to use electrical impedance tomography (EIT) to measure the blood pressure pulses directly within the descending aorta, but it required at least 32 impedance electrodes placed around the chest at the level of the axilla, which prevented it from the routine clinical practice. In contrast, the Generalized Transfer Function (GTF) method, which applies a transfer function for CAP derivation and related aortic hemodynamic indices extraction, has attracted extensive research interest in the past decade (?). Although there are already several commercial products, such as SphygmoCor and HEM-9000AI, which are widely used in the clinical environment, how to determine the transfer function, particularly the specific transfer function for different subjects remains a challenge. ? further simplified the idea of a general function and proposed a simple N-Point Moving Average (NPMA), mathematically a low pass filter, to non-invasively derive CAP from the radial artery pressure waveform. Both the GTF-CAP or NPMA-CAP methods can be used for noninvasive assessment of central aortic pressure indices, but they ignore the individual differences in terms of blood viscosity, fluid inertia and arterial compliance, which may cause significant CAP errors.

To take the individual differences into consideration and improve the CAP estimation accuracy, it is critical to model the arteries. In general, the arteries can be modeled as a 0D-model, 1D-model, 2D-model and 3D-model (?). The 3D and 2D models are widely applied for the analysis of local blood flow. For example, ? applied a 3D-model to study blood flow circulation in intracranial arterial networks. ? explored the pulsating turbulent phenomena in stenotic vessels. A 1D-model of the blood flow in deformable vessels has been proven to be a simple and effective approach to simulate the hemodynamics of the vascular system, which has been widely used for systematic arterial network modeling (?). For example, ? applied

TABLE I: The subjects detailed information  
(Sex, Age, Systolic blood pressure, Diastolic blood pressure and Diabetes)

	Sex	Age	SBP(mmHg)	DBP(mmHg)	Diabetes
No.1	F	85	136	58	No
No.2	M	60	117.4	64.5	Yes
No.3	M	62	112.7	65.1	Yes
No.4	F	59	128.6	57.6	No
No.5	M	57	125.6	47.8	Yes
No.6	F	70	107.7	69.5	Yes
No.7	M	71	129.9	63	No
No.8	M	63	116.4	81.2	Yes
No.9	F	55	152.4	59.8	Yes
No.10	M	62	155.4	73.8	No
No.11	F	56	137.3	62.5	Yes
No.12	M	66	117.5	68.1	Yes
No.13	M	63	106.5	53.3	Yes
No.14	F	70	144.6	67.9	Yes
No.15	F	73	146	67.4	No
No.16	M	58	142.3	78.4	Yes
No.17	M	54	133.5	71.9	Yes
No.18	F	62	101.9	59.2	No
Mean±SD		63.7±7.7	128.4±16.2	65.0±8.5	
Range	56%(M)	54~85	101.9~155.4	47.8~81.2	66.7%(Y)

a 1D-model to compare the pressure and flow wave propagation in conduit arteries against a well-defined experimental 1:1 replica of the human arterial tree, which consisted of 37 silicone branches representing the largest central systemic arteries in the human. ? proposed a simple lumped parameter model for the heart and showed how it could be coupled numerically with a 1D model of the arteries. However, 1D-models requires defined of vessel parameters, such as vessel radius, blood density and wall thickness, in advance which can't be acquired non-invasively. Unlike a 1D-model which reduces the vessel space dependence to the vessel axial coordinate only, 0D-models discretize the space dependence by splitting the cardiovascular system into a set of compartments, and uses an equivalent electric circuit to describe the arbitrary length and structure of blood vessels( ?? ), which can significantly reduce the complexity of the vascular modeling, but it can't describe the geometrical structure of arteries network in the 0D-model.

Considering the state-of-the-art for non-invasive CAP estimation and vascular system modeling, we present a personalized-model-based central aortic pressure estimation method (PM-CAP) in this paper. The main contributions of the paper are:

- Personalized artery network model: The vessels are mathematically modeled based on hydrodynamics with the continuity and the momentum equations. This model method is more thorough than the Windkessel model method. The model parameters can be personalized: via measuring the pulse wave at the proximal and distal ends of the radial artery, the least square method is then proposed to estimate the model parameters.
- Personalized transfer function and CAP waveform estimation: a Subject-specific ascending aorta-radial artery transfer function can then be acquired to obtain the continuous central artery blood pressure waveform.

An invasive validation study with 18 subjects comparing PM-CAP with direct aortic root pressure measurements during percutaneous transluminal coronary intervention was carried out at the Beijing Hospital. The experimental results have shown accurate CAP estimations can be acquired with regard to the invasive measurements for all the subjects, which illustrates the feasibility and effectiveness of the proposed method.

The remainder of the paper is organized as follows. Section II presents the viscous fluid mechanics based arteries model, the patient-specific parameter estimation and CAP estimation. Experimental results and conclusion are then provided in Section III and IV.

## II. PM-CAP METHOD

### A. Data Acquisition

18 subjects (10 males, 8 females) were recruited (Table I). All volunteers gave written informed consent approved by the Institutional Review Board at Beijing Hospital before participating. Direct aortic root pressure waveforms were collected during percutaneous transluminal coronary intervention by inserting a 6FR angiography catheter (Cordis Corporation) into the right radial artery, and the catheter was connected to the commercial Mac-Lab hemodynamic recording system (GE Healthcare). Meanwhile, pulse waveforms at the proximal and distal ends of the radial artery were also measured by catheter, which is used to estimate radial artery model parameters in the Section II.D.

## B. Human Arteries Modeling

Human arteries are composed of finite but very small vessels and they can be divided into large arteries and small arteries according to the radius. In this section, we will introduce these two types of arteries separately.

1) *Large arteries*: As shown in the Fig.2, any large artery  $\Omega^l$  of length  $l$  can be modeled as  $N$  finite but very small vessels  $\Omega_1^{l,\Delta l}$ ,  $\Omega_2^{l,\Delta l}$  ... and  $\Omega_N^{l,\Delta l}$  with the same properties; therefore, we can assume cross-sectional area  $A_0$ ; blood viscosity,  $\eta$ , blood density  $\rho$ , vascular thickness  $h_0$ , Young's modulus  $E$ , average blood flow  $\hat{Q}(t)$  and average blood pressure  $\hat{P}(t)$  are constant. Thus according to Equation (34) the fluid dynamics equations of large artery can then be simplified as:

$$\begin{cases} C \frac{dP(t)}{dt} + Q(t, x_e) - Q(t, x_s) = 0 \\ L \frac{dQ(t)}{dt} + RQ(t) + P(t, x_e) - P(t, x_s) = 0 \end{cases} \quad (1)$$

where  $C = \frac{2l\sqrt{A_0}}{\beta}$  is arterial compliance,  $L = \rho l/A_0$  is the fluid inertia,  $R = \frac{8\eta l}{\pi r_0^4}$  is blood resistance. However, similar equations can also be found in the analysis of electric circuits, thus we can simulate the flow in the vascular system based on analog electric circuits. In the electric network analogy, the blood flow  $Q$  and blood pressure  $P$  are equivalent to the current and voltage, while arterial compliance, blood inertia and blood resistance correspond to capacitance, inductance and resistance; therefore, the corresponding circuit can be derived as shown in Fig.3.

2) *Small arteries*: Similar to the large arteries, we can define a small artery as  $\Omega^M$  as  $N$  finite but very small vessels  $\Omega_1^{M,\Delta l}$ ,  $\Omega_2^{M,\Delta l}$  ... and  $\Omega_N^{M,\Delta l}$ , then we obtain the similar fluid dynamics equations as:

$$\begin{cases} C^M \frac{dP^M(t)}{dt} + Q^M(t, x_e) - Q^M(t, x_s) = 0 \\ L^M \frac{dQ^M(t)}{dt} + R^M Q^M(t) + P^M(t, x_e) - P^M(t, x_s) = 0 \end{cases} \quad (2)$$

where  $C^M$  is the compliance,  $L^M$  is the fluid inertia,  $R^M$  is the blood resistance,  $Q^M$  is the blood flow and  $P^M$  is the blood pressure. Since  $\frac{dP^M(t)}{dt}$  and  $\frac{dQ^M(t)}{dt}$  are very small in small arteries, they can be ignored, thus we can simplify the above equations to:

$$\begin{cases} Q^M(t, x_e) - Q^M(t, x_s) = 0 \\ R^M Q^M(t) + P^M(t, x_e) - P^M(t, x_s) = 0. \end{cases} \quad (3)$$

Similarly, the corresponding circuit can be obtained as shown in Fig.4. In practice, we always take the resistance  $R^M$  in small arteries as the peripheral resistance, and use symbol  $RP^M$  to represent it.

## C. Human Arteries Network Model

Human body has 55 large arteries and 28 small arteries. This division was originally introduced by ? and the data of diameter, length, wall, thickness and Youngs modulus of 55 largest arteries was introduced by ?. Using the electric circuit in Fig.3 to represent large arteries and the electric circuit in Fig.4 to represent small arteries, the human arterial network can be abstracted as a network of electric circuits consisting of capacitance, inductance and resistance, as shown in Fig.5. Due to space constrictions, here we only present the circuit between the left radial artery and ascending aorta, the whole body circuit given at the end of this paper(Appendix B). To estimate the BP at point  $A$  from the BP measurement at point  $B$  and  $C$ , the circuit parameters need to be estimated first.

## D. Patient-Specific Parameters Estimation

To determine the patient-specific parameters for the human artery network as shown in Fig.5, we need to estimate: 1)  $RP_i$ , where  $i = 1, 2, \dots, 28$ , 2)  $L_j$ ,  $C_j$  and  $R_j$ , where  $j = 1, 2, \dots, 55$ . Via measuring the pulse wave of the proximal and distal ends of the radial artery:  $P_{22}(t, x_s)$  and  $P_{22}(t, x_e)$ , we will introduce how to estimate them separately.

1) *Estimate Peripheral Resistances  $RP_i$* : On the basis of 0D theory,  $R + RP = P/CO$  ( $P$  is the average central aortic pressure,  $CO$  is cardiac output,  $R$  is total large artery resistance, and  $RP$  is total small artery resistance). Then we have 2 assumption that: (1)the average BP at central artery is equal to the average BP at the proximal end of radial artery [1]; (2)because of the radius of small arteries is less then the radius of large arteries, the  $RP$  is widely larger then the  $R$  ( see the expression for  $R$ , Equation (18)), ignore the  $R$ . Then  $R + RP = P/CO$  is simplified to:

$$RP \approx \frac{\bar{P}_{22}(x_s)}{CO} \quad (4)$$

where  $\bar{P}_{22}(x_s)$  is the average BP at the proximal end of radial artery over period  $T$ , which can be calculated as

$$\bar{P}_{22}(x_s) = \frac{1}{T} \int_0^T P_{22}(t, x_s) dt. \quad (5)$$

122  $CO$  is the cardiac output, which is given as ?:

$$CO = \frac{17}{K^2}(P_{22}^s - P_{22}^d) \quad (6)$$

123 where  $P_{22}^s$  and  $P_{22}^d$  are the measured systolic and diastolic blood pressure at the proximal end of radial artery respectively,  
124 and  $K$  is the pulse contour characteristic value as ?

$$K = \frac{\bar{P}_{22}(x_s) - P_{22}^d}{P_{22}^s - P_{22}^d}. \quad (7)$$

125 The relationship between  $RP_i$  and the total peripheral resistance  $RP$  can be written as:

$$\frac{1}{RP_i} = \frac{1}{RP} - \sum_k \frac{1}{RP_k} \quad (8)$$

126 where  $k = 1, 2, \dots, 28$  and  $k \neq i$ . Denote the ratio  $w_k^{RP}$  as  $\frac{RP}{RP_k}$ , then we can get

$$\frac{1}{RP_i} = \frac{RP}{1 - \sum_k \frac{RP}{RP_k}} = \frac{RP}{1 - \sum_k w_k^{RP}}. \quad (9)$$

127 Here, the ratio  $w_k^{RP}$  can be assumed to be constant for different subjects to simplify the derivation process, and they can be  
128 acquired in advance ?.

129 2) *Estimate Left Radial Artery Model Parameters(The least squares method):*  $R_{22}$ ,  $C_{22}$  and  $L_{22}$ : To simplify the analysis,  
130 the left radial artery model is shown separately in Fig.6, where  $R_{22}$ ,  $L_{22}$ ,  $C_{22}$  are its resistance, inductance and capacitance,  
131 respectively;  $P_{22}(t, x_s)$ ,  $P_{22}(t, x_e)$ ,  $Q_{22}(t, x_s)$  and  $Q_{22}(t, x_e)$  are blood pressures and flows in the both ends of radial artery  
132 respectively.

133 From the radial artery model shown in Fig.6, we can obtain the following equations:

134

$$\begin{cases} P_{22}(t, x_e) = Q_{22}(t, x_e)RP_{22} \\ \frac{dP_{22}(t, x_e)}{dt} = \frac{Q_{22}(t, x_s) - Q_{22}(t, x_e)}{C_{22}} \\ \frac{dQ_{22}(t, x_s)}{dt} = \frac{P_{22}(t, x_s) - P_{22}(t, x_e) - Q_{22}(t, x_s) \cdot R_{22}}{L_{22}} \end{cases} \quad (10)$$

135

136 get the below equation from Equation (10):

$$\begin{aligned} L_{22}C_{22}RP_{22} \frac{d^2 Q_{22}(t, x_e)}{dt^2} + (L_{22} + R_{22}C_{22}RP_{22}) \\ \cdot \frac{dQ_{22}(t, x_e)}{dt} + (RP_{22} + R_{22})Q_{22}(t, x_e) = P_{22}(t, x_s). \end{aligned} \quad (11)$$

137 Take any  $N$  sets of measurements  $P_{22}(t, x_s)$ ,  $P_{22}(t, x_e)$  from  $t = t_1, t_2 \dots t_N$ , we can have

$$P_{22,N} = H_N \theta \quad (12)$$

138 where

$$P_{22,N} = \begin{bmatrix} P_{22}(t_1, x_s) \\ P_{22}(t_2, x_s) \\ \vdots \\ P_{22}(t_N, x_s) \end{bmatrix}, \quad (13)$$

139

$$\begin{aligned} \theta &= [\theta_1, \theta_2, \theta_3]^T \\ &= [L_{22}C_{22}RP_{22}, L_{22} + R_{22}C_{22}RP_{22}, RP_{22} + R_{22}]^T \end{aligned} \quad (14)$$

140 and

$$H_N = \begin{bmatrix} \frac{d^2 Q_{22}(t_1, x_e)}{dt^2} & \frac{dQ_{22}(t_1, x_e)}{dt} & Q_{22}(t_1, x_e) \\ \frac{d^2 Q_{22}(t_2, x_e)}{dt^2} & \frac{dQ_{22}(t_2, x_e)}{dt} & Q_{22}(t_2, x_e) \\ \vdots & \vdots & \vdots \\ \frac{d^2 Q_{22}(t_N, x_e)}{dt^2} & \frac{dQ_{22}(t_N, x_e)}{dt} & Q_{22}(t_N, x_e) \end{bmatrix} \quad (15)$$

141 so we can get  $\hat{\theta}$  as:

$$\hat{\theta} = (H_N^T H_N)^{-1} H_N^T P_{22,N}. \quad (16)$$

142 Thus  $R_{22}$ ,  $C_{22}$  and  $L_{22}$  can be calculated as:

$$\begin{cases} R_{22} = \hat{\theta}_3 - RP_{22} \\ C_{22} = \frac{\hat{\theta}_2 RP_{22} + \sqrt{(\hat{\theta}_2 RP_{22})^2 - 4\hat{\theta}_1 R_{22} (RP_{22})^2}}{2R_{22} (RP_{22})^2} \\ L_{22} = \hat{\theta}_2 - C_{22} R_{22} RP_{22}. \end{cases} \quad (17)$$

143 The solution about estimating left radial artery model parameters is that: Firstly, the peripheral resistance of radial artery  
144  $RP_{22}$  could be calculated by equation (4) to (9). Secondly, the blood flow at the end of radial artery  $Q_{22}(t, x_e)$  in equation(15)  
145 could be calculated by the first equation of equation set (10):  $Q_{22}(t, x_e) = P_{22}(t, x_e)/RP_{22}$ . It means that, we use the  
146 pressure of proximal and distal ends of radial artery :  $P_{22}(t, x_s)$  and  $P_{22}(t, x_e)$  to estimate the  $R_{22}$ ,  $C_{22}$ ,  $L_{22}$  of radial artery  
147 by equation (16) and (17).

148 3) *Estimate Other large Arteries Parameters:  $R_j$ ,  $C_j$  and  $L_j$*  : For any  $j$ th ( $j = 1, 2, 3 \dots, 55$ ) large artery in the Fig.5, the  
149  $C_j$ ,  $R_j$  and  $L_j$  can be defined as ?:

$$\begin{aligned} C_j &= \frac{2l_j \sqrt{A_{0,j}}}{\beta_j} \\ R_j &= \frac{8\eta l_j}{\pi r_i^4} \\ L_j &= \frac{\rho l_j}{A_{0,j}}. \end{aligned} \quad (18)$$

150 where

$$\beta_j = \frac{\sqrt{\pi} h_{0,j} E_j}{(1-\nu^2) A_{0,j}}. \quad (19)$$

151 Define

$$\begin{aligned} \omega_j^A &= A_{0,j}/A_{0,22} \\ \omega_j^l &= l_j/l_{22} \\ \omega_j^r &= r_j/r_{22} \\ \omega_j^h &= h_{0,j}/h_{0,22} \\ \omega_j^E &= E_j/E_{22} \end{aligned} \quad (20)$$

152 Then we can have:

$$\begin{cases} C_j = C_{22} \cdot \frac{l_j \sqrt{A_j} \beta_{22}}{l_{22} \sqrt{A_{22}} \beta_j} = \frac{C_{22} \omega_j^l (\sqrt{\omega_j^A})^3}{\omega_j^h \omega_j^E} \\ R_j = R_{22} \frac{l_j / (r_j)^4}{l_{22} / (r_{22})^4} = R_{22} \omega_j^l / (\omega_j^r)^4 \\ L_j = L_{22} \frac{l_j / A_{0,i}}{l_{22} / A_{0,22}} = L_{22} \omega_j^l / \omega_j^A. \end{cases} \quad (21)$$

153 Similar to  $\omega_i^{RP}$ ,  $\omega_j^A$ ,  $\omega_j^l$ ,  $\omega_j^r$ ,  $\omega_j^h$  and  $\omega_j^E$  are also constant for different subjects, and they can be acquired in advance(?).

### 154 E. CAP Estimation

155 Once all the parameters in the Fig.5 are known, it is straightforward to calculate the impulse response function  $H(t)$  between  
156 the radial arterial blood pressure  $P_{22}(t, x_e)$  and central aortic blood pressure  $CAP(t)$ (?), and the central aortic pressure can  
157 then be estimated as

$$CAP(t) = H(t) \otimes P_{22}(t, x_e) \quad (22)$$

158 where  $\otimes$  represents the convolution operation.

## 159 III. EXPERIMENTAL RESULTS AND DISCUSSION

160 To better illustrate the performance of our method, we compared the estimated CAP with the ground-truth measured from  
161 the catheter during percutaneous transluminal coronary intervention. For analysis purpose, the comparison between our method  
162 and the state-of-the-art non-invasive methods, such as GTF-CAP and NPMA-CAP, are also conducted in this section.

### 163 A. CAP waveform estimation results

164 Central aortic waveforms contain valuable cardiovascular information, for example, the rising phases of the waveforms  
 165 reflects the myocardial contractility, while the descending phases illustrate the timing of aortic valve closure; therefore, it is  
 166 critical to recover the CAP waveforms. In our first experiment, parameter values of the radial artery and the blood pressure  
 167 waveforms of the central artery were estimated, which are given in the Table II and Fig.7. In the Fig.7, the black solid lines  
 168 indicate the direct invasive measurements as the ground-truth, the red dashed lines represent our estimations, while the blue  
 169 dotted lines and green dotted-dashed lines are the estimated waveforms by the GTF-CAP and NPMA-CAP, respectively.

170 The GTF-CAP and NPMA-CAP measures were obtained by collected the blood pressure at the distal end of the radial artery  
 171 by inserting a 6FR angiography catheter (Cordis Corporation), which is connected to the commercial Mac-Lab hemodynamic  
 172 recording system(GE Healthcare), into the right radial artery at Beijing Hospital. The GTF method ( ?) to estimate the central  
 173 artery pressure: (1)Get the general transfer function which is calculated by a large number of clinical experiment data ( ?):  
 174 radial artery pressure/aortic artery pressure. (2)Blood pressure÷ GTF to estimate the central artery pressure. Thirdly, we used  
 175 NPMA( ?) method to estimate the central artery pressure: use n-point moving average method which acts as a low pass filter  
 176 to smooth collected blood pressure data(  $n = \text{sampling frequency} / 4$ , the value is 256 in this article).

177 As we can see from the Fig.7, it is obvious that our proposed method can get more accurate CAP waveforms for different  
 178 subjects compared to the GTF-CAP and NPMA-CAP methods. The main reason is we estimated subject-specific parameters in  
 our method, which could handle the individual differences ignored by both GTF-CAP and NPMA-CAP methods. As shown in

TABLE II: The parameter values of the radial artery subjects.  
 (the oldest and youngest males and females)

ID	L	C	R	RP
	$(mmHg \cdot sec^2/ml)(ml/mmHg)(mmHg \cdot sec/ml)(mmHg \cdot sec/ml)$			
1(oldest female)	0.0482	0.0029	2.988	79.95
7(oldest male)	0.0248	0.0036	0.839	43.02
5(youngest male)	0.0936	0.0012	2.402	54.06
9(youngest female)	0.0121	0.0011	4.076	62.57

179 the Table II, it is evident that there are significant artery parameters differences for subjects, and ignorance of such individual  
 180 differences should be avoided during the CAP estimation. Although there are no ground-truth values for the artery parameters,  
 181 we insist it is still worthwhile to take the individual differences into consideration and try to get more accurate CAP waveform  
 182 estimation. The above qualitative analysis has shown that the proposed CAP estimation method can significantly improve the  
 183 accuracy of the central arterial waveforms over the existing non-invasive methods. To further illustrate the strength of the  
 184 proposed method over the GTF-CAP and NPMA-CAP methods, quantitative analysis was also conducted. Here, root-mean-  
 185 square error(RMSE)mean error and standard deviation, and correlation coefficient were used as the evaluation standards: the  
 186 estimated CAP and invasive measured CAP are time-varying waveforms, then we sampled 150 data points of them by 15Hz  
 187 frequency and subtract a point-by-point value of computed method from measured value to get errors. Lastly, calculate the  
 188 root-mean-square error, mean error, standard deviation and correlation coefficient. Results are shown in the Fig.8(a), Fig.8(b),  
 189 and Fig.8(c) respectively. As we can see from the figures, our method can achieve the smallest RMSE and high correlation  
 190 coefficient values for all the subjects. We also noticed the correlation coefficient values of the GTF-CAP methods are slightly  
 191 better than those of our method for some certain subjects, but the differences are very small and the RMSE of GTF-CAP are  
 192 much larger for those subjects. It illustrates that the overall performance of our method is better than those of GTF-CAP and  
 193 NPMA-CAP methods.

### 195 B. Systolic and diastolic blood pressure estimation results

196 Since the central aortic systolic and diastolic blood pressure are important indicators to measure the level of high blood  
 197 pressure, we also statistically analyzed the central systolic blood pressure and diastolic blood pressure as shown in the Fig.9.  
 198 The average errors for central aortic systolic blood pressure estimation are  $1.4165mmHg$ ,  $6.4140mmHg$  and  $7.7991mmHg$   
 199 for our method, NPMA-CAP and GTF-CAP, respectively, while the standard deviations of the errors are  $5.8558mmHg$ ,  
 200  $8.1155mmHg$  and  $8.5936mmHg$ . The average errors for central aortic diastolic blood pressure estimation are  $2.1413mmHg$ ,  
 201  $9.4160mmHg$  and  $3.7646mmHg$  for our method, NPMA-CAP and GTF-CAP, respectively, while the standard deviations of  
 202 the errors are  $3.6420mmHg$ ,  $4.3795mmHg$  and  $4.2777mmHg$ . It is evident that our proposed method can achieve the most  
 203 accurate and stable systolic and diastolic blood pressure estimations, and they are also consistent with the standard of the  
 204 Association for the Advancement of Medical Instrumentation (mean error less than 5 mmHg and standard deviation less than  
 205  $8mmHg$ )( ?).

### 206 C. Discussion

207 Above subsections show that PM-CAP method could estimate more accurate CAP waveform for different subjects compared  
 208 to the GTF-CAP and NPMA-CAP method. Let us insight these three method. See the error analysis of transfer function of

209 them (Table III). It shows that the error of PM-CAP transfer function 0-5Hz is less than the errors of GTF-CAP transfer  
 210 function and NPMA-CAP transfer function. ? tell us that the power spectral density of blood pressure wave mainly distribute  
 211 in the 0-5 Hz. Obviously, the main reason that PM-CAP method is more accurate than other two method is PM-CAP method  
 212 used subjected-specific parameters. Then the transfer function between CAP(central aortic pressure) to RAP(radial artery blood  
 213 pressure) of different subjects is personalized and more close to real transfer function.

TABLE III: Error Analysis of Transfer Function

	Mean difference(0-2Hz)	Mean difference(2-5Hz)
PM-CAP	0.0744	0.1548
GTF-CAP	0.1630	2.4375
NPMA-CAP	0.1144	2.2553

214 However, there are also some certain errors between our estimations and the direct invasive measurements.

215 The experiment uses invasive methods to obtain radial artery blood pressure for checking the validity of the artery model.  
 216 In general application scenario, we can use the pressure sensor to collect non-invasive radial arterial blood pressure waveform  
 217 , and use korotkoff sounds method to obtain radial artery blood pressure for calibrating the blood pressure waveform. The  
 218 korotkoff sounds method has difficult to obtain the accurate blood pressure, which will affect the accuracy of the pressure  
 219 value estimation, but this does not affect the accuracy of waveform estimation.

220 Although we have tried our best in the experiment to synchronize all the measurements, there was still some delay between  
 221 the pulse waves of the proximal and distal ends of the radial artery, which caused the errors in the model parameters estimation  
 222 and thus the error in the CAP waveform estimations. Meanwhile, to simplify the derivation and make the model computable,  
 223 we have made some approximations in the arteries network modeling and assumed  $w_i^{RP}$ ,  $\omega_j^A$ ,  $\omega_j^l$ ,  $\omega_j^r$ ,  $\omega_j^h$  and  $\omega_j^E$  were constant  
 224 for different subjects. In normal condition, such assumption is valid and robust. However, such proportional constants may/may  
 225 not change duo external stimulations, such as drugs, which needs to be further verified. Due to the experimental constraints for  
 226 this pilot study, we didn't take such condition into consideration. In the near future, when we carry out large scale studies,  
 227 we will explore the robustness of such assumption, and more rigorous tests on more subjects under different situations will be  
 228 carried out.

#### 229 IV. CONCLUSION

230 In this paper, we present a personalized-model-based central aortic pressure estimation method (PM-CAP) (PM-CAP). PM-  
 231 CAP has mathematical foundation: a novel human aortic network model is proposed and developed based on viscous fluid  
 232 mechanics theory. Via measuring the pulse wave of the proximal and distal ends of the radial artery, the least square method  
 233 was then proposed to estimate the patient-specific circuit parameters. Thus the central aortic pulse wave was then obtained  
 234 via calculating the transfer function between radial artery and central aortic. An invasive validation study with 18 subjects  
 235 comparing M-CAP with direct aortic root pressure measurements during coronary intervention were carried out at the Beijing  
 236 Hospital. The experimental results have shown better performance of PM-CAP method compared to the GTF-CAP method and  
 237 NPMA-CAP method, which illustrated the feasibility and effectiveness of the proposed method. In the future, more subjects'  
 238 data will be collected and analyzed to further evaluate the proposed method. The exploration the relationship between the blood  
 239 vessel parameters and cardiovascular disease will also be carried out. [Conflict of interest]The authors declared that they have  
 240 no conflicts of interest to this work. We declare that we do not have any commercial or associative interest that represents a  
 241 conflict of interest in connection with the work submitted

242 [Conflict of interest]The authors declared that they have no conflict of interest to this work. We declare that we do not have  
 243 any commercial or associative interest that represents a conflict of interest in connection with the work submitted.

#### 244 REFERENCES

- 245 Alpert B, Friedman B, Osborn D. Aami blood pressure device standard targets home use issues. Home Healthcare Horizons  
 246 2010;:69–72.
- 247 Chen CH, Nevo E, Fetics B, Pak PH, Yin FCP, Maughan WL, Kass DA. Estimation of central aortic pressure waveform  
 248 by mathematical transformation of radial tonometry pressure. validation of generalized transfer function. Circulation  
 249 1997;95(7):1827–36.
- 250 Dorf RC, Bishop RH. Modern control systems. Pearson, 2011.
- 251 Fetics B, Nevo E, Chen C, Kass D. Parametric model derivation of transfer function for noninvasive estimation of aortic  
 252 pressure by radial tonometry. Biomedical Engineering, IEEE Transactions on 1999;46(6):698–706.
- 253 Formaggia L, Lamponi D, Tuveri M, Veneziani A. Numerical modeling of 1d arterial networks coupled with a lumped  
 254 parameters description of the heart. Computer methods in biomechanics and biomedical engineering 2006;9(5):273–88.
- 255 Formaggia L, Quarteroni AM, Veneziani A. Cardiovascular Mathematics: Modeling and simulation of the circulatory system.  
 256 volume 1. Springer:New York, 2009.

- 257 Grinberg L, Cheever E, Anor T, Madsen J, Karniadakis G. Modeling blood flow circulation in intracranial arterial networks:  
 258 a comparative 3D/1D simulation study. *Annals of biomedical engineering* 2011;39(1):297–309.
- 259 Hopcroft MA, Nix WD, Kenny TW. What is the Young's Modulus of silicon? *Microelectromechanical Systems, Journal of*  
 260 *2010;19(2):229–38.*
- 261 Luo ZC, Zhang S, Yang YM. *Pulse Wave Engineering Analysis and Clinical Application*. Beijing: Science Press, 2006.
- 262 Matthys K, Alastruey J, Peiró J, Khir A, Segers P, Verdonck P, Parker K, Sherwin S. Pulse wave propagation in a model  
 263 human arterial network: Assessment of 1-D numerical simulations against in vitro measurements. *Journal of biomechanics*  
 264 *2007;40(15):3476–86.*
- 265 O'Rourke MF, Seward JB. Central arterial pressure and arterial pressure pulse: new views entering the second century after  
 266 korotkov. In: *Mayo Clinic Proceedings*. Elsevier; volume 81; 2006. p. 1057–68.
- 267 Reymond P. *Pressure and Flow Wave Propagation in Patient-Specific Models of the Arterial Tree*. Ph.D. thesis; École  
 268 Polytechnique FÉDÉRALE De Lausanne; 2011.
- 269 Reymond P, Merenda F, Perren F, Rüfenacht D, Stergiopoulos N. Validation of a one-dimensional model of the systemic arterial  
 270 tree. *American Journal of Physiology-Heart and Circulatory Physiology* 2009;297(1):H208–22.
- 271 Riha K, Benes R. Testing of methods for artery section area detection 2011;.
- 272 Riha K, Chen P, Fu D. Detection of artery section area using artificial immune system algorithm. In: *Proceedings of the 7th*  
 273 *conference on Circuits, systems, electronics, control and signal processing*. 2008. p. 46–52.
- 274 Solà J, Adler A, Santos A, Tusman G, Sipmann FS, Bohm SH. Non-invasive monitoring of central blood pressure by electrical  
 275 impedance tomography: first experimental evidence. *Medical & biological engineering & computing* 2011;49(4):409–15.
- 276 Stergiopoulos N, Meister JJ, Westerhof N. Simple and accurate way for estimating total and segmental arterial compliance: the  
 277 pulse pressure method. *Annals of biomedical engineering* 1994;22(4):392–7.
- 278 Stergiopoulos N, Young D, Rogge T. Computer simulation of arterial flow with applications to arterial and aortic stenoses.  
 279 *Journal of biomechanics* 1992;25(12):1477–88.
- 280 Tsanas A, Goulermas J, Vartela V, Tsiapras D, Theodorakis G, Fisher A, Sfirakis P. The windkessel model revisited: A  
 281 qualitative analysis of the circulatory system. *Medical engineering & physics* 2009;31(5):581–8.
- 282 Varghese SS, Frankel SH. Numerical modeling of pulsatile turbulent flow in stenotic vessels. *Transactions-American Society*  
 283 *Of Mechanical Engineers Journal Of Biomechanical Engineering* 2003;125(4):445–60.
- 284 Wang J, Parker K. Wave propagation in a model of the arterial circulation. *Journal of biomechanics* 2004;37(4):457–70.
- 285 Westerhof N, Bosman F, De Vries CJ, Noordergraaf A. Analog studies of the human systemic arterial tree. *Journal of*  
 286 *biomechanics* 1969;2(2):121–43.
- 287 Westerhof N, Lankhaar J, Westerhof B. The arterial windkessel. *Medical and Biological Engineering and Computing*  
 288 *2009;47(2):131–41.*
- 289 Williams B, Lacy P, Thom S, Cruickshank K, Stanton A, Collier D, Hughes A, Thurston H, O'Rourke M, et al. Differential  
 290 impact of blood pressure-lowering drugs on central aortic pressure and clinical outcomes. *Circulation* 2006;113(9):1213–25.
- 291 Williams B, Lacy P, Yan P, Hwee C, Liang C, Ting C. Development and validation of a novel method to derive central aortic  
 292 systolic pressure from the radial pressure waveform using an N-point moving average method. *Journal of the American*  
 293 *College of Cardiology* 2011;57(8):951–61.
- 294 Zamir M. *Modelling preliminaries. The Physics of Coronary Blood Flow* 2005;:35–77.

## APPENDIX A

### A FINITE BUT VERY SMALL VESSEL MODEL

297 The blood vessel  $\Omega^l$  can be defined as an elastic tube as shown in the Fig.1, where  $l$  is the length,  $v$  is the volume,  $A(t, x)$   
 298 is the cross-sectional area at time  $t$  and location  $x$  along the vessel axis,  $r(t, x)$  is radius,  $u(t, x)$  is blood velocity,  $\rho(t, x)$  is  
 299 the blood density,  $\eta(t, x)$  is the blood viscosity,  $Q(t, x)$  is blood flow and  $P(t, x)$  is blood pressure. If the length of  $\Omega^l$  is finite  
 300 but very small, i.e.  $l = \Delta l$ , the blood viscosity  $\eta^{\Delta l}$ , velocity  $u^{\Delta l}$  and density  $\rho^{\Delta l}$  will be constant, and the cross-sectional  
 301 area along the vessel axis will also be constant as  $A^{\Delta l}(t) = A^{\Delta l}(t, x)$ , thus  $\Omega^l$  can then be regarded as the finite but very  
 302 small vessel, denoted by  $\Omega^{\Delta l}$ . In general, blood has been conceptualized as a viscous fluid; therefore, it should follow the  
 303 laws of conservation of mass and momentum, which can be described by the basic equations of fluid dynamics: the continuity  
 304 equation and momentum equation, respectively( ? ).

305 1) *Continuity equation*: The continuity equation for vessel  $\Omega^l$  can be defined as:

$$\frac{\partial A(t)}{\partial t} + \frac{\partial Q(t, x)}{\partial x} = 0 \quad (23)$$

306 the continuity equation for vessel  $\Omega^{\Delta l}$  can then be written as:

$$\Delta l \frac{dA^{\Delta l}(t)}{dt} + Q^{\Delta l}(t, x_e) - Q^{\Delta l}(t, x_s) = 0 \quad (24)$$

307 where  $x_s$  and  $x_e$  are the starting and ending locations of vessel  $\Omega^{\Delta l}$  respectively. According to the vessel wall mechanics( ? ),  
 308 the blood pressure in  $\Omega^{\Delta l}$  can be calculated as

$$P^{\Delta l}(t, x) = P_{ext}^{\Delta l}(t, x) + \beta^{\Delta l}(\sqrt{A^{\Delta l}(t)} - \sqrt{A_0^{\Delta l}}) \quad (25)$$

309 where  $P_{ext}^{\Delta l}(t, x)$  is the external pressure on the vessel wall,  $A_0^{\Delta l}$  is the initial cross-sectional area when there is now blood  
 310 flow in the vessel, and  $\beta^{\Delta l}$  is a coefficient which can be defined as:

$$\beta^{\Delta l} = \frac{\sqrt{\pi} h_0^{\Delta l} E^{\Delta l}}{0.75 A_0^{\Delta l}} \quad (26)$$

311 where  $h_0^{\Delta l}$  is the thickness of the wall and  $E^{\Delta l}$  is the Young's modulus( ? ). Integrate Equation(26) along the axis of the  
 312 blood vessel and differentiate with respect to time.

$$\int_{x_s}^{x_e} \frac{\partial P^{\Delta l}(t, x)}{\partial t} dx = \int_{x_s}^{x_e} \frac{\beta^{\Delta l}}{2\sqrt{A^{\Delta l}(t)}} \frac{\partial A^{\Delta l}(t)}{\partial t} dx. \quad (27)$$

313 Some papers show that the section area of artery is changed by only 10% ( ?? ), therefor we assume  $A_0^{\Delta l} \approx A^{\Delta l}(t)$  for the  
 314 vessel  $\Omega^{\Delta l}$  , so the average pressure  $\hat{P}^{\Delta l}(t)$  should satisfy:

$$\frac{d\hat{P}^{\Delta l}(t)}{dt} = \frac{\beta^{\Delta l}}{2\sqrt{A_0^{\Delta l}}} \frac{dA^{\Delta l}(t)}{dt}. \quad (28)$$

315 where

316

$$\hat{P}^{\Delta l} = \frac{\int_{x_s}^{x_e} P^{\Delta l}(x) dx}{\Delta l} \quad (29)$$

317

318

Substituting (28) into (24), we can get:

$$\frac{2\Delta l \sqrt{A_0^{\Delta l}}}{\beta^{\Delta l}} \frac{d\hat{P}^{\Delta l}(t)}{dt} + Q^{\Delta l}(t, x_e) - Q^{\Delta l}(t, x_s) = 0. \quad (30)$$

319

2) *Momentum equation*: The momentum equation for vessel  $\Omega^l$  can be written as:

$$\begin{aligned} \frac{\partial Q(t, x)}{\partial t} + \frac{\partial}{\partial x} \left( \frac{Q(t, x)^2}{A(t, x)} \right) + \frac{A(t, x)}{\rho(t, x)} \cdot \frac{\partial P(t, x)}{\partial x} \\ + \frac{8u(t, x)\eta(t, x)A(t)}{\rho(t, x)r(t)^2} = 0. \end{aligned} \quad (31)$$

320

321

For the vessel  $\Omega^{\Delta l}$ , the above equation can be simplified as

$$\begin{aligned} \rho^{\Delta l} \int_{x_s}^{x_e} \frac{\partial Q^{\Delta l}(t)}{\partial t} dx + A^{\Delta l}(t) \int_{x_s}^{x_e} \frac{\partial P^{\Delta l}(t, x)}{\partial x} dx \\ + \frac{8u^{\Delta l}\eta^{\Delta l}A^{\Delta l}(t)}{(r^{\Delta l}(t))^2} \int_{x_s}^{x_e} dx = 0. \end{aligned} \quad (32)$$

322

323

324

As  $A_0^{\Delta l} \approx A^{\Delta l}(t)$ , the equation (32) can be simplified as:

$$\begin{aligned} \frac{\rho^{\Delta l} \Delta l}{A_0^{\Delta l}} \cdot \frac{d\hat{Q}^{\Delta l}(t)}{dt} + \frac{8\eta^{\Delta l} \Delta l}{A_0^{\Delta l} (r_0^{\Delta l})^2} \hat{Q}^{\Delta l}(t) \\ + P^{\Delta l}(t, x_e) - P^{\Delta l}(t, x_s) = 0. \end{aligned} \quad (33)$$

325

326

327

According to the Zamir's definitions( ? ) and Equation(30) arterial compliance  $C^{\Delta l}$ , blood resistance  $R^{\Delta l}$  of the vessel  $\Omega^{\Delta l}$  can then be written as:

$$\begin{aligned} C^{\Delta l} &= \frac{d\Delta V^{\Delta l}(t)}{d\hat{P}^{\Delta l}(t)} = \frac{\Delta Q^{\Delta l}(t) dt}{d\hat{P}^{\Delta l}(t)} = \frac{Q^{\Delta l}(t, x_s) - Q^{\Delta l}(t, x_e)}{d\hat{P}^{\Delta l}(t)/dt} \\ &= \frac{2\Delta l \sqrt{A_0^{\Delta l}}}{\beta^{\Delta l}} \end{aligned}$$

$$R^{\Delta l} = \frac{8\eta^{\Delta l}\Delta l}{\pi(r_0^{\Delta l})^4} = \frac{8\eta^{\Delta l}\Delta l}{A_0^{\Delta l}(r_0^{\Delta l})^2}$$

329 Fluid inertia  $L^{\Delta l}$  means the ratio of force difference (include 2 forces: one is the pressure of blood and the other is the  
330 viscous force of blood) and flow rate variation ratio. Therefore,  $L^{\Delta l}$  is:

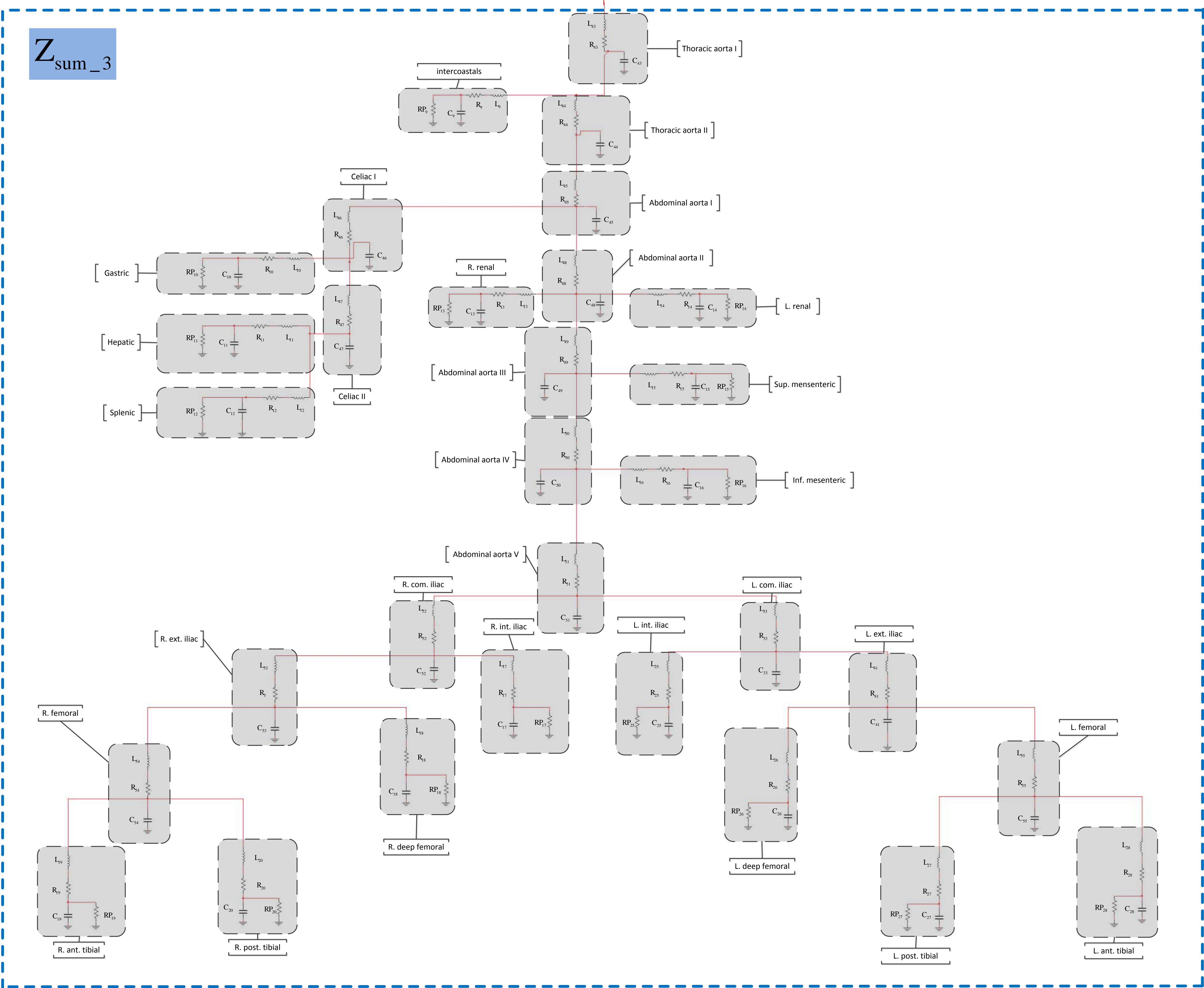
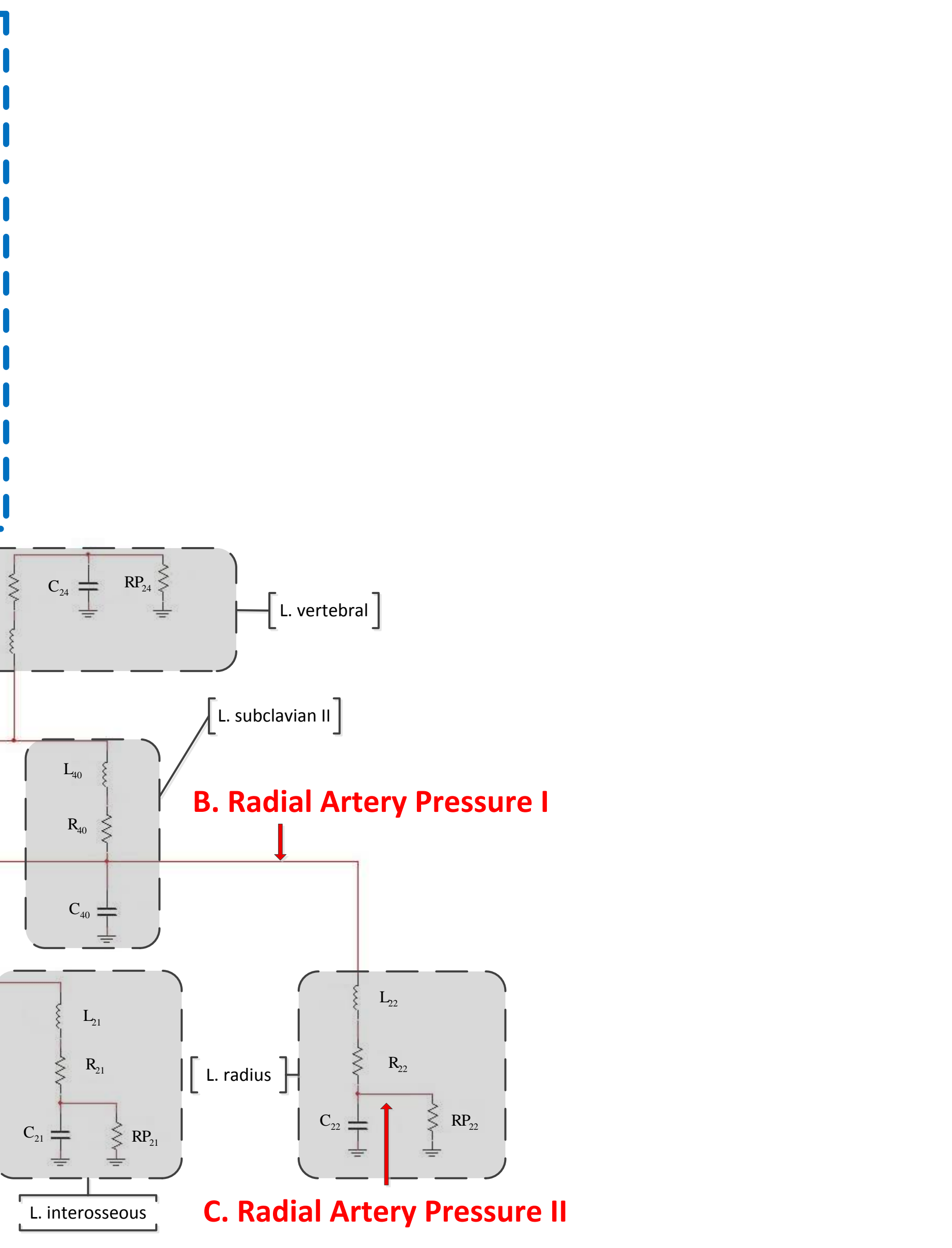
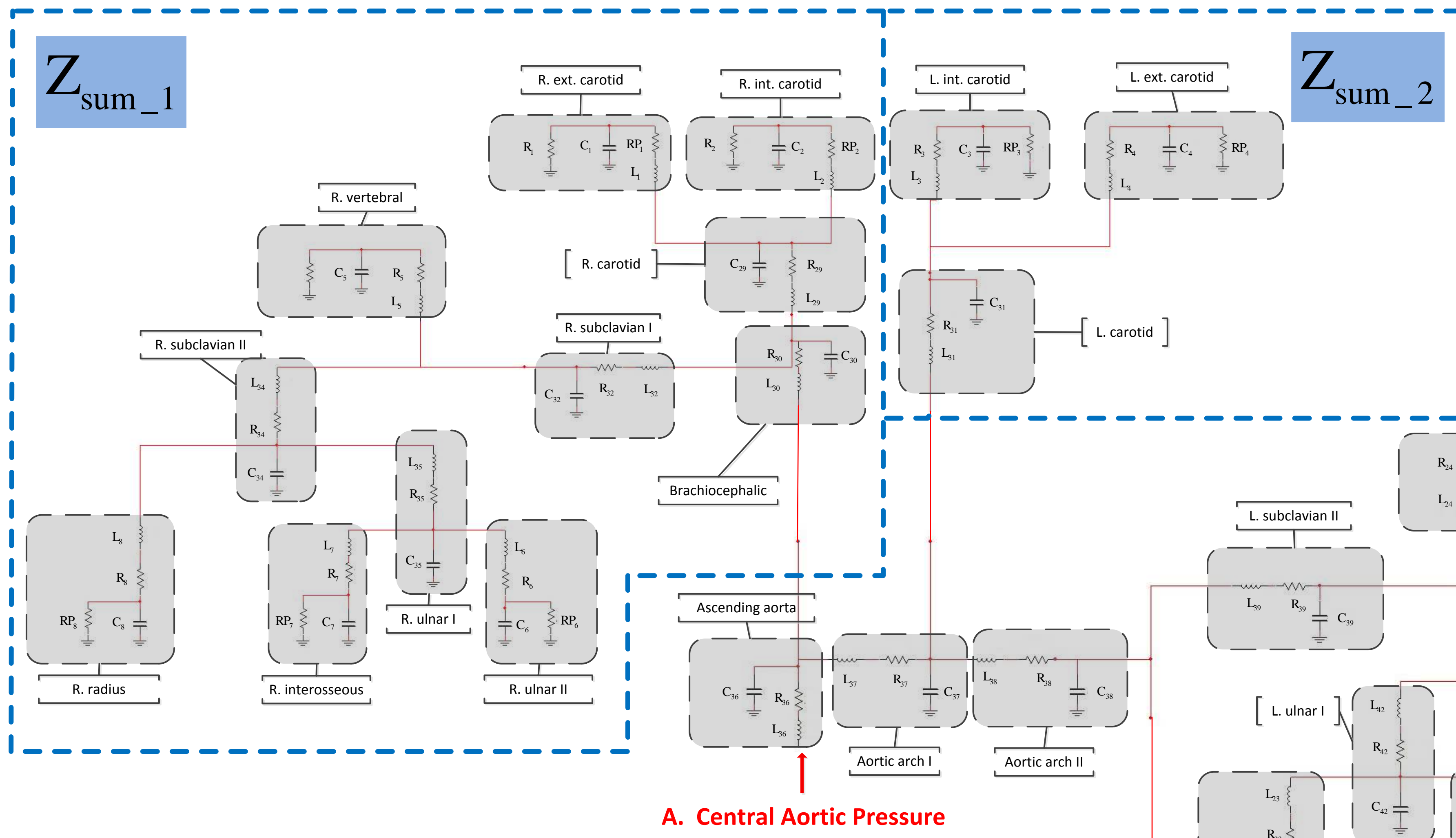
$$L^{\Delta l} = \frac{\frac{8\eta^{\Delta l}\Delta l}{A_0^{\Delta l}(r_0^{\Delta l})^2}\hat{Q}^{\Delta l}(t) + P^{\Delta l}(t, x_e) - P^{\Delta l}(t, x_s)}{d\hat{Q}^{\Delta l}(t)/dt} = \frac{\rho^{\Delta l}\Delta l}{A_0^{\Delta l}}$$

331 respectively. Therefore, the equations (30) and (33) can be simplified as

$$\begin{cases} C^{\Delta l} \frac{d\hat{P}^{\Delta l}(t)}{dt} + Q^{\Delta l}(t, x_e) - Q^{\Delta l}(t, x_s) = 0 \\ L^{\Delta l} \frac{d\hat{Q}^{\Delta l}(t)}{dt} + R^{\Delta l} \hat{Q}^{\Delta l}(t) + P^{\Delta l}(t, x_e) - P^{\Delta l}(t, x_s) = 0. \end{cases} \quad (34)$$

332  
333

## APPENDIX B B:HUMAN ARTERIES NETWORK MODEL



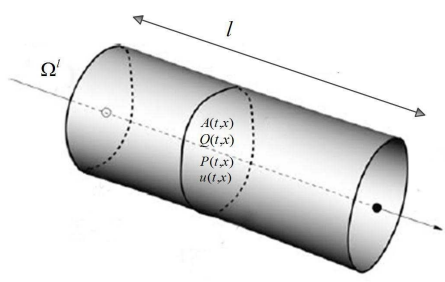


Fig. 1: The illustration of the elastic vessel

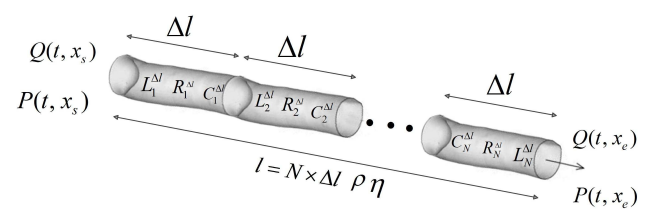


Fig. 2: The illustration of a segment of large artery

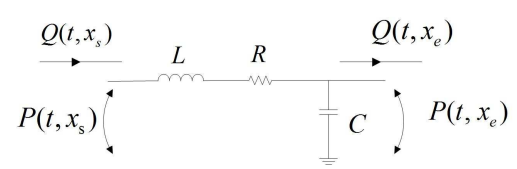


Fig. 3: The large artery model.

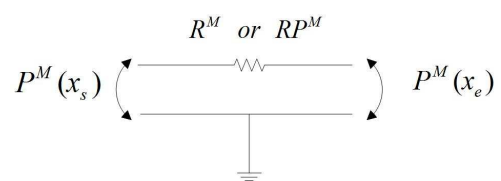


Fig. 4: The small artery model.

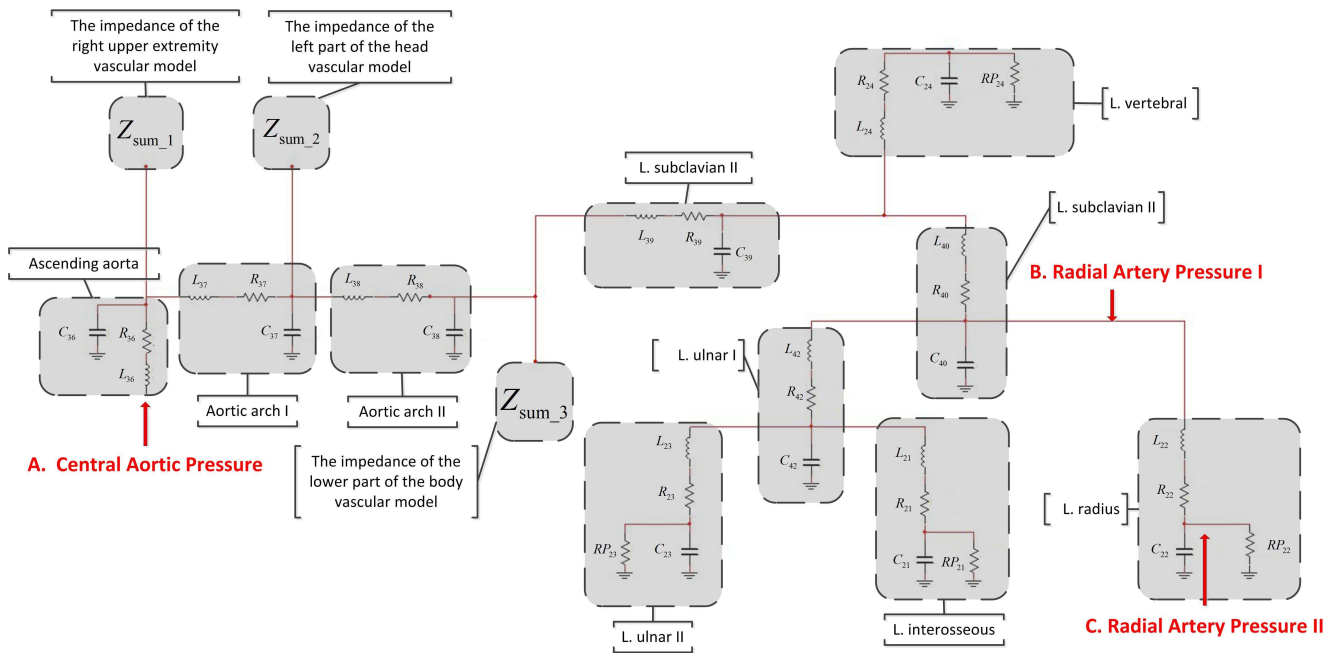


Fig. 5: The corresponding electric circuit between left radial artery and ascending aorta. Point B and C are the proximal and distal ends of the radial artery, where the BP can be measured conveniently. Point A is the starting point of central aorta, where the BP is about to estimate.

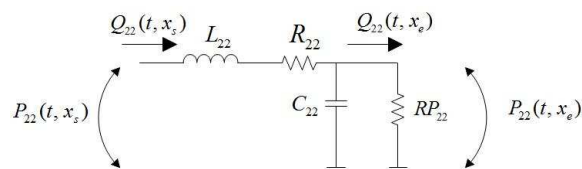
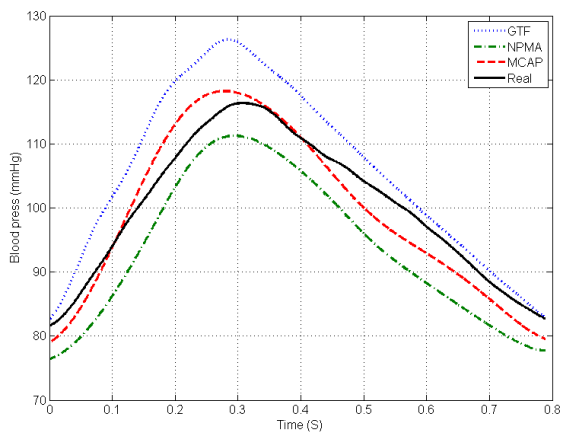
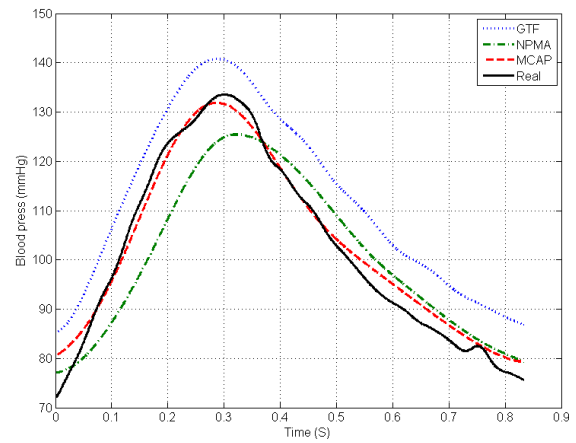


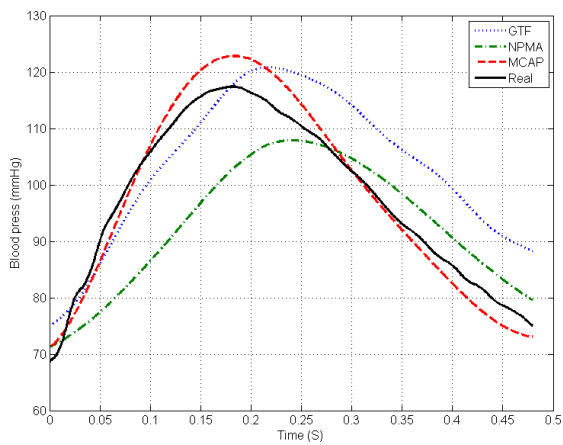
Fig. 6: The left radial artery model



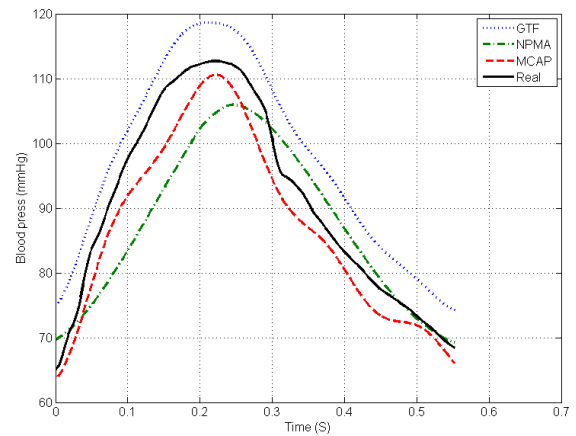
(a)



(b)

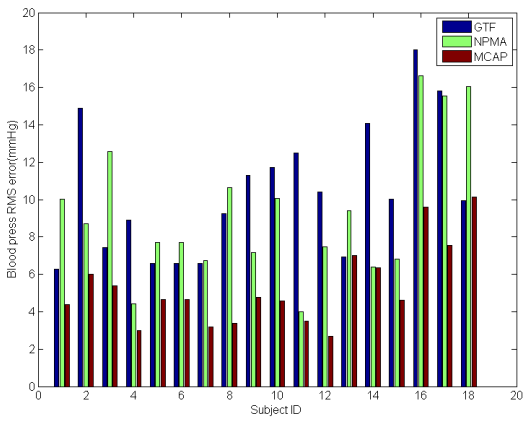


(c)

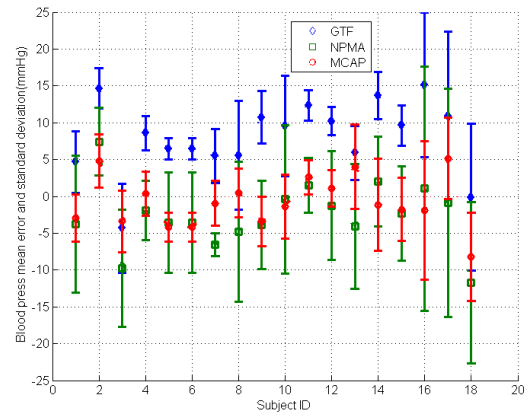


(d)

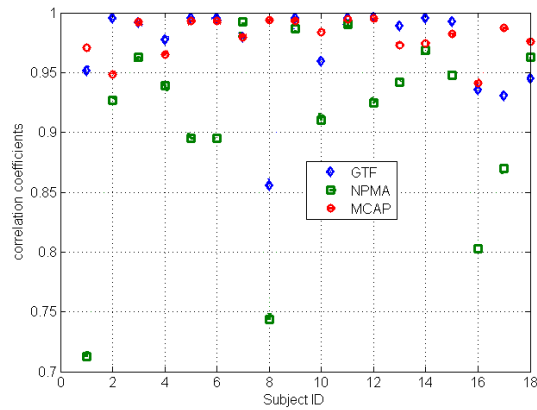
Fig. 7: The estimated blood pressure waveforms of the central aorta. Here, we randomly selected 4 subjects, and they are (a) subject ID 1, (b) subject ID 7, (c) subject 5, (d) subject 9.



(a) RMSE



(b) Mean and standard deviation (SD)



(c) correlation coefficient

Fig. 8: quantitative analysis results. (a) The RMSE comparison among our method, GTF-CAP and NPMA-CAP methods; (b) The mean error and standard deviation comparison among our method, GTF-CAP and NPMA-CAP methods; (c) the correlation coefficient values comparison among our method, GTF-CAP and NPMA-CAP methods.

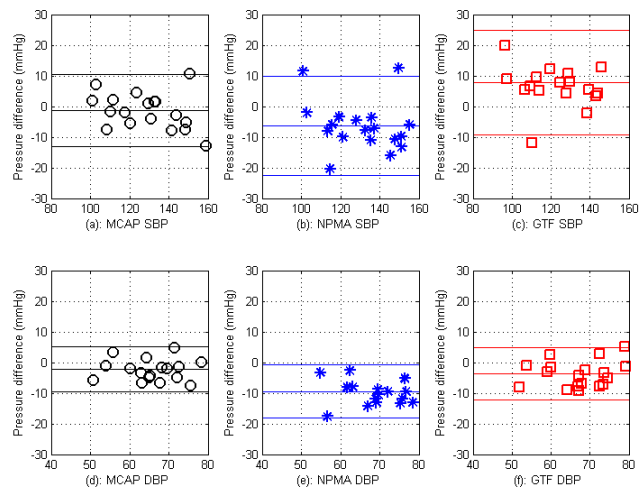


Fig. 9: Bland-Altman analysis of central aortic systolic and diastolic blood pressure. The three horizontal lines on each sub-figure indicate:  $\text{mean} + 2 * SD$ , mean, and  $\text{mean} - 2 * SD$ . (a) systolic blood pressure comparison between our proposed method and ground-truth; (b) systolic blood pressure comparison between NPMA-CAP and ground-truth; (c) systolic blood pressure comparison between GTF-CAP and ground-truth; (d) diastolic blood pressure comparison between our proposed method and ground-truth; (e) diastolic blood pressure comparison between NPMA-CAP and ground-truth; (f) diastolic blood pressure comparison between GTF-CAP and ground-truth.